

Towards understanding the doping mechanism of organic semiconductors by Lewis acids

Brett Yurash¹, David Xi Cao¹, Viktor V. Brus¹, Dirk Leifert¹, Ming Wang¹, Alana Dixon¹, Martin Seifrid¹, Ahmed E. Mansour³, Dominique Lungwitz³, Tuo Liu⁴, Peter J. Santiago¹, Kenneth R. Graham¹, Norbert Koch¹, Guillermo C. Bazan¹ and Thuc-Quyen Nguyen¹

Precise doping of organic semiconductors allows control over the conductivity of these materials, an essential parameter in electronic applications. Although Lewis acids have recently shown promise as dopants for solution-processed polymers, their doping mechanism is not yet fully understood. In this study, we found that $B(C_6F_5)_3$ is a superior dopant to the other Lewis acids investigated (BF_3 , BBr_3 and $AlCl_3$). Experiments indicate that Lewis acid-base adduct formation with polymers inhibits the doping process. Electron-nuclear double-resonance and nuclear magnetic resonance experiments, together with density functional theory, show that p-type doping occurs by generation of a water-Lewis acid complex with substantial Brønsted acidity, followed by protonation of the polymer backbone and electron transfer from a neutral chain segment to a positively charged, protonated one. This study provides insight into a potential path for protonic acid doping and shows how trace levels of water can transform Lewis acids into powerful Brønsted acids.

he ability to precisely and controllably dope inorganic semi-conductors is the underpinning of modern electronics. This provides much of the motivation behind the long-standing interest in doping of organic semiconductors. As early as 1977, it was shown that the conductivity of polyacetylene can be controlled over 11 orders of magnitude by vapour doping using volatile halogens, such as $\rm I_2$ (ref. 1). However, this method of doping suffers from a practical viewpoint: reproducibility, bulk homogeneity and stability present substantial obstacles to commercial implementation.

Several years later, it was discovered that Brønsted acids, such as hydrogen fluoride and trifluoroacetic acid (TFA), were able to effectively p-dope polyacetylene, as well as many other organic semiconducting polymers^{2,3}. The majority of the mechanisms proposed invoke the double protonation of a polymer chain, followed by an internal redox process to produce either bipolarons or singly charged polarons⁴⁻⁷. However, identification and characterization of protonated intermediates and the resulting radical species have remained elusive.

Just before the turn of the present century, controllable molecular p-doping of organic semiconductors was realized by co-sublimation of phthalocyanine derivatives with 2,3,5,6-tetrafluoro-7,7,8,8-tetracyanoquinodimethane (F_4TCNQ)8. This doping mechanism proceeds by integer charge transfer (ICT) from the highest occupied molecular orbital (HOMO) of the semiconductor to the lowest unoccupied molecular orbital of the dopant, introducing a hole (polaron) on the semiconductor while simultaneously creating a negatively charged dopant anion9. Since this discovery, numerous studies have demonstrated that molecular p-doping is a viable strategy for modulation of charge transport and charge injection in opto-electronic devices 10-14.

The success of F₄TCNQ as a molecular dopant has remained, for the most part, limited to processing by thermal evaporation. Using F₄TCNQ in solution-processed organic semiconductors has been plagued with problems that typically derive from the markedly different solubilities of the organic semiconductor, neutral F₄TCNQ and the F₄TCNQ anion¹⁴⁻¹⁷. Moreover, the ability to p-dope materials possessing a large HOMO energy necessitates the design of molecular dopants with even greater electron-accepting ability, which is no simple task.

A growing body of literature indicates that tris (pentafluor ophenyl) borane (B(C_6F_5)₃), hereafter referred to as BCF, represents a promising class of p-type dopant for organic semiconductors, due to its excellent solubility in common organic solvents and its ability to dope materials of relatively large ionization potential (~5.8 eV)¹⁸⁻²¹. Besides their ability to p-dope certain semiconductors, Lewis acids are also known to form Lewis acid-base adducts with Lewis basic semiconductors, which changes the electronic structure of the semiconductor and markedly decreases the optical gap of the semiconductor ²²⁻²⁵. Despite all of these studies, the precise mechanism of Lewis acid doping remains elusive and the relationship between adduct formation and doping remains unknown.

Here, we systematically investigate how a range of Lewis acids affect the opto-electronic properties of semiconducting polymers with varying degrees of Lewis basicity. Electrical measurements demonstrate that BCF is the best dopant of the Lewis acids tested, even surpassing the performance of F₄TCNQ in the case of one polymer. A combination of spectroscopic techniques indicates that Lewis acid-base adduct formation inhibits the doping process. Subsequent investigation into the doping mechanism of BCF via magnetic resonance techniques, in conjunction with density functional theory (DFT) calculations, reveals that doping occurs by (1) formation of a strongly (Brønsted) acidic BCF-H₂O complex, (2) protonation of 4,4-dihexadecyl-4*H*-cyclopenta[1,2-*b*:5,4-*b*'] dithiophene (CPDT) moieties and (3) electron transfer from a neutral polymer chain segment to a protonated one.

¹Center for Polymers and Organic Solids, Department of Chemistry and Biochemistry, University of California, Santa Barbara, CA, USA. ²Center for Advanced Low-Dimension Materials, Donghua University, Shanghai, China. ³Institut für Physik & IRIS Adlershof, Humboldt-Universität zu Berlin, Berlin, Germany. ⁴Department of Chemistry, University of Kentucky, Lexington, KY, USA. *e-mail: bazan@chem.ucsb.edu; quyen@chem.ucsb.edu

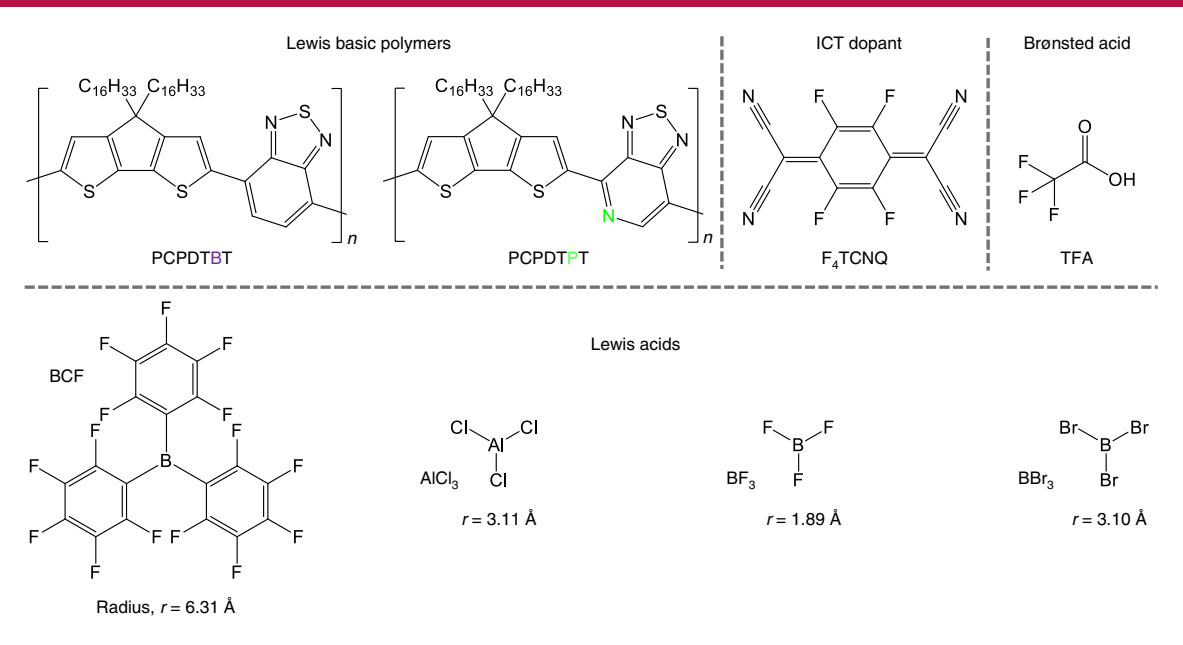


Fig. 1 | Chemical structures of the polymers studied, and the various molecules used to dope them. The relative acidity of the four Lewis acids increases from left to right, AlCl₃ being approximately equal to BF₃ (ref. ⁴⁶). The relative size (radius, r) of the Lewis acids is also shown, as estimated from DFT-optimized geometries. The regionegularity of PCPDTPT (not shown here, for simplicity) is shown in Supplementary Fig. 1.

The chemical structures of poly[2,6-(4,4-bis(2-hexadecyl)-4Hcyclopenta [2,1-b;3,4-b'] dithiophene) - alt-4,7(2,1,3-benzothiadiazole)] (PCPDTBT) and poly[2,6-(4,4-bis(2-hexadecyl)-4H-cyclopenta[2,1-b;3,4-b']dithiophene)-alt-4,7-(4,4-dihexadecvl-4H-cyclopenta[2,1-b:3,4-b']dithiophene-2,6-divl)bis([1,2,5] thiadiazolo[3,4-c]pyridine)] (PCPDTPT) are shown in Fig. 1, along with the chemical structures of the dopants used in this work. Figure 2 shows the electrical properties of PCPDTPT (left panels) and PCPDTBT (right panels) with various dopants. Conductivity $(\sigma, \text{ Fig. 2a,b})$ was measured for films deposited on interdigitated gold contacts, whereas the free charge carrier (hole) density (p, Fig. 2c,d) was determined from impedance spectroscopy measurements on devices with the metal-insulator-semiconductor (MIS) architecture (see Methods and Supplementary Fig. 2 for further details). Impedance spectroscopy could be performed only for relatively small dopant concentrations, because at higher concentrations the thickness of the depletion region becomes so small that the total capacitance of the MIS structures is almost totally determined by the insulator capacitance (in the equivalent circuit model, the depletion layer capacitor and the insulator capacitor are connected in series) and, therefore, it is not possible to determine the carrier density at high-doping concentrations.

Doping efficiencies (Fig. 2e,f) were determined by considering how many holes were generated per molecule of dopant added. Hole mobility, μ_p , (Fig. 2g,h) was then determined from the equation for conductivity, $\sigma = qp\mu_p$ where q is the elementary charge.

As shown in Supplementary Fig. 3, because boron trifluoride (BF₃) does not substantially dope PCPDTPT we did not pursue electrical measurements of this combination. Despite the reasonable doping efficiency when added to PCPDTBT, overall conductivity was not greatly improved with BF₃ due to a substantial reduction in hole mobility. It is important to note that, to obtain accurate control of the concentration of BF₃ in these experiments, it had to be added in the form of liquid BF₃ diethyl etherate, unlike BCF which can be readily handled as a pure solid at room temperature. For these reasons we decided to focus our subsequent efforts on the Lewis acid BCF.

The doping efficiency of BCF when added to PCPDTPT was found to be quite low (<2%). Only at the two highest concentrations

studied was the conductivity enhancement of PCPDTPT with BCF superior to F_4 TCNQ. This can be attributed to (1) negligible changes in hole mobility with F_4 TCNQ compared to substantial increase in hole mobility with increasing BCF concentration, and (2) negligible changes in the doping efficiency of BCF with concentration compared to the rapid decrease in F_4 TCNQ with increasing concentration.

In PCPDTBT, the doping efficiency of BCF was found to be superior to that of $\rm F_4TCNQ$, reaching a maximum of 14.6% at 0.010 molar equivalents. Conductivity with BCF was superior to enhancements by $\rm F_4TCNQ$, and only at the two lowest concentrations was hole mobility with BCF lower than that with $\rm F_4TCNQ$. In Supplementary Fig. 4 we show that the conductivity of PCPDTBT can be improved over four orders of magnitude with BCF, reaching a maximum conductivity of $\rm 8\times10^{-3}\,S\,cm^{-1}$ with 0.200 molar equivalents.

To investigate the effect of BCF on polymer morphology and molecular packing, we performed atomic force microscopy (AFM; Supplementary Figs. 5 and 6) and grazing incidence wide-angle X-ray scattering (GIWAXS; Supplementary Figs. 7–10) on pristine and doped thin films. No substantial changes in π – π stacking distances or surface roughness were observed, suggesting that the performance of BCF as a dopant is not limited by a detrimental impact on polymer morphology. This is in stark contrast to F₄TCNQ, which is known to aggregate in films and disrupt the molecular packing of the host semiconductor 14–16.

To confirm that the enhanced electrical properties of the polymers following the addition of BCF are attributable to p-type doping, we investigated the contact resistance of films with, and without, BCF (Supplementary Fig. 11). Contact resistance was found to be negligible in all cases. In addition, we studied the effect of BCF on polymers via ultraviolet photoelectron spectroscopy (UPS). These measurements revealed a marked increase in work function of both polymers following the addition of BCF, while the ionization potential remained essentially constant (Supplementary Figs. 12 and 13), which is the expected behaviour for p-type doping $^{26-28}$. In addition, the ionization potential of both pristine PCPDTPT (4.9 eV) and pristine PCPDTBT (4.7 eV) is sufficiently low to expect ICT from F_4 TCNQ (Supplementary Fig. 14), whose electron affinities in the

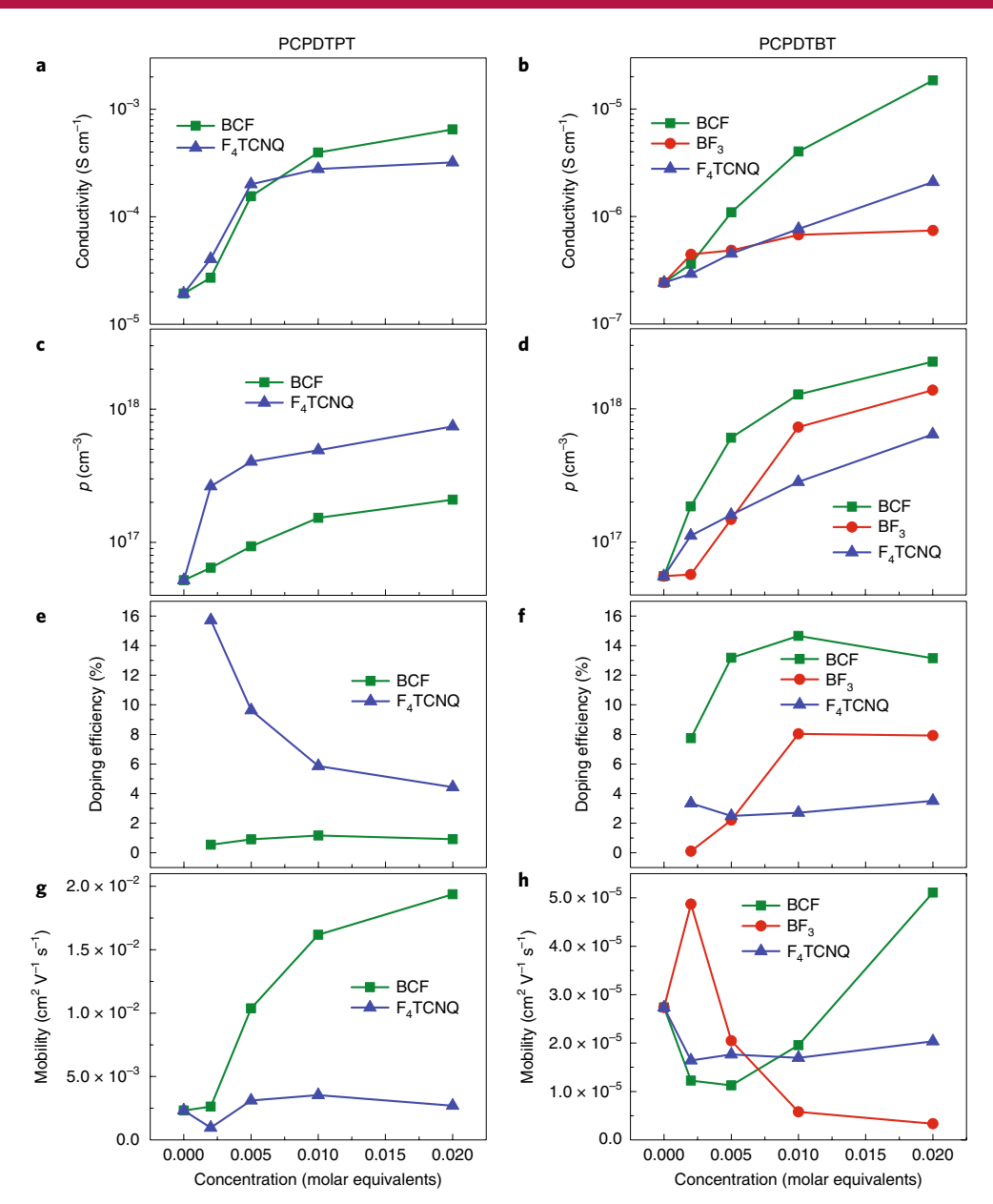


Fig. 2 | Electrical characteristics of PCPDTPT and PCPDTBT with varying amounts of dopant. a,b, Conductivity of PCPDTPT (a) and PCPDTBT (b). c,d, Free charge carrier density (p) for PCPDTPT (c) and PCPDTBT (d). e,f, Doping efficiency for PCPDTPT (e) and PCPDTBT (f). g,h, Hole mobility for PCPDTPT (g) and PCPDTBT (h). The concentration of dopants is given in molar equivalents with respect to the polymer repeat unit.

solid state and in acetonitrile solution are both approximately 5.2 eV (refs. ^{13,29}). We believe that the possibility of ICT to BCF is unlikely for the following reasons: (1) the lowest unoccupied molecular orbital level of BCF, as measured by cyclic voltammetry in dichloromethane, is 3.01 eV, markedly different from the HOMO level of most organic semiconductors; and (2) not even metallic sodium or potassium can reduce BCF³⁰⁻³².

Next, we sought to investigate the relationship between doping and Lewis acid adduct formation in the solid state via ultraviolet-visible-near infrared (UV-Vis-NIR) absorption spectroscopy, electron paramagnetic resonance (EPR) spectroscopy and X-ray photoelectron spectroscopy (XPS). As shown in Fig. 3a, there is considerable adduct formation between BCF and PCPDTPT as evidenced by the appearance of the new nitrogen 1s binding peak at approximately 401 eV. In contrast, an insignificant amount of adduct formation was observed between PCPDTBT and BCF (Fig. 3b).

XPS survey, high-resolution C1s and high-resolution S2p spectra are shown in Supplementary Fig. 15.

Figure 3c shows how the addition of BCF resulted in a clear decrease in the PCPDTPT optical gap, red-shifting the absorption maximum by 0.37 eV. Interestingly, the EPR signal intensity (Fig. 3e) from films with 2.0 molar equivalents of BCF was lower than that with 1.0 molar equivalents of BCF, a trend that coincides with the intensity of absorption around 1,500 and 3,000 nm. As such, we attribute these regions of NIR absorption to polaron absorption and conclude that, at high concentrations of BCF and despite increased adduct formation, doping is suppressed. In fact, at a high concentration of BCF in solution (8.0 molar equivalents), no doping was observed despite clear adduct formation (Supplementary Fig. 16). To further verify that adduct formation is not responsible for doping, we added the stronger Lewis acid boron tribromide (BBr₃) to PCPDTPT, where we observed adduct formation but no doping (Supplementary Fig. 17).

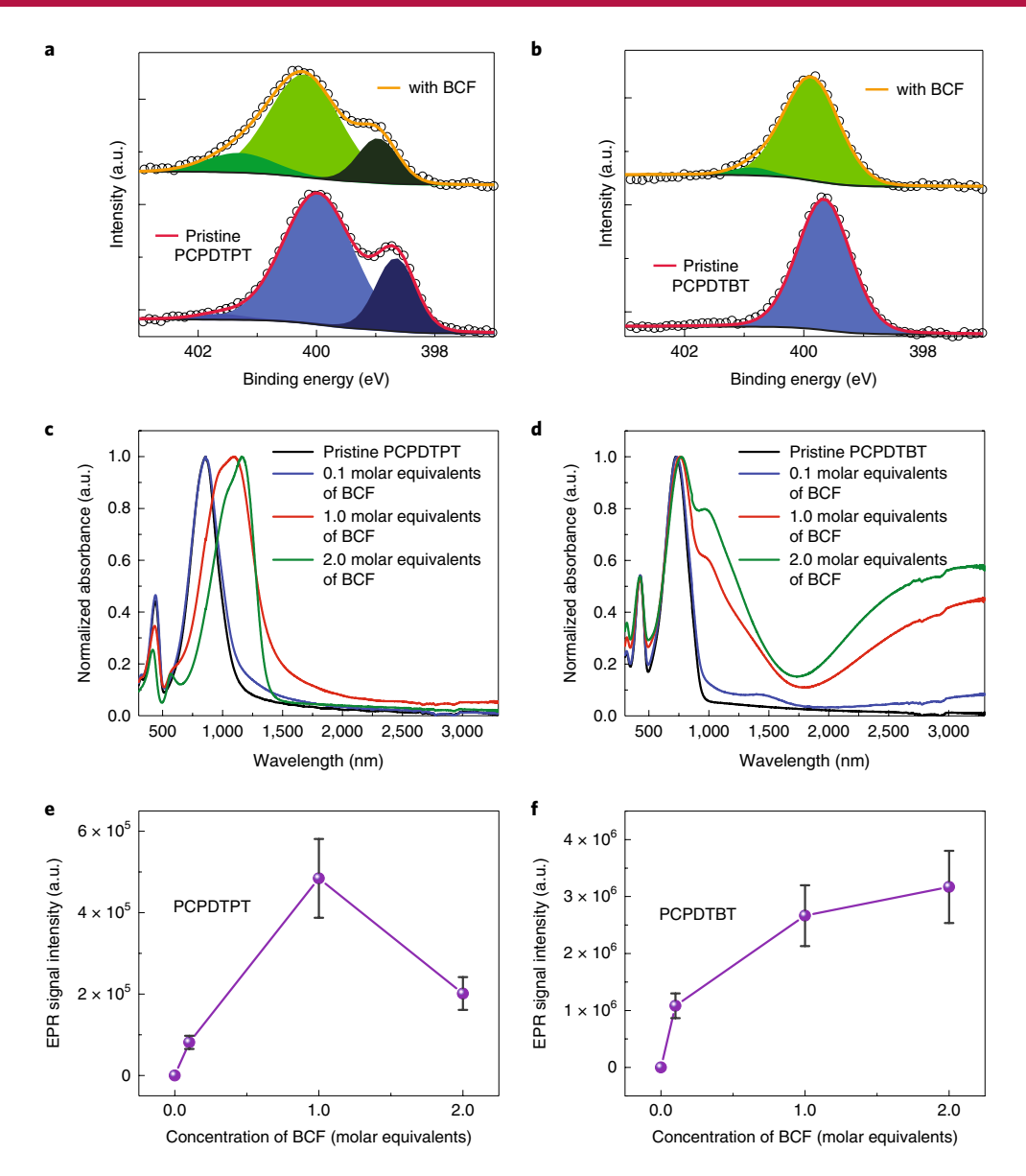


Fig. 3 | Thin-film properties of PCPDTPT and PCPDTBT with Lewis acid BCF. a,b, XPS N 1s of PCPDTPT (**a**) and PCPDTBT (**b**) with 1.0 molar equivalents of BCF. Solid lines are the result of fitting raw data (open circles) to Voigt profiles. Individual peak areas determined from the fitting procedure are indicated by different shades of the same colour. a.u., arbitrary units. **c,d**, Absorption of PCPDTPT (**c**) and PCPDTBT (**d**) with BCF. **e,f**, EPR signal intensity of PCPDTPT (**e**) and PCPDTBT (**f**) with BCF at the same microwave power (1.002 μW). An error of 20% was included to reflect potential differences in sample volume and Q values (see Methods for sample preparation details).

On the other hand, the absorption spectrum of PCPDTBT (Fig. 3d) is marked by a monotonic increase in polaron absorption (1,100- and 3,000-nm regions), coinciding with a monotonic increase in EPR signal intensity (Fig. 3f). In light of the XPS measurements (Fig. 3b and Supplementary Fig. 18), we conclude that BCF is able to dope PCDTBT to high levels without forming a Lewis acid-base adduct with the polymer.

Our final investigation into the electronic structure of polymer films doped with BCF was performed through inverse photoemission spectroscopy (IPES; Supplementary Fig. 19). From these measurements we were able to determine the effect of BCF on the transport gap. The results are in excellent agreement with changes in the optical gap, indicating that (1) PCPDTBT is heavily doped by BCF and (2) adduct formation with PCPDTPT results in a 0.4-eV increase in ionization potential and a 0.8-eV increase in electron affinity (0.4-eV reduction in the transport gap). The marked increase in the ionozation potential of PCPDTPT with BCF may

account for the loss of doping effects following increased adduct formation, since protonation becomes increasingly difficult for materials with higher ionization potential. Alternatively, the added steric bulk of the adduct may have precluded the doping process.

The observation that adduct formation inhibits the doping process readily explains the trends in doping efficiency for the two Lewis basic polymers. The doping efficiency of BCF is higher for PCPDTBT than for PCPDTPT, because the latter polymer has stronger Lewis basic sites, specifically pyridyl nitrogen atoms, which are conducive to adduct formation. Similarly, the doping efficiency of BF3 is higher for PCPDTBT than for PCPDTPT (for which there was an unsubstantial amount of doping). Because BF3 is a stronger and smaller Lewis acid than BCF, it was expected to bind more easily with Lewis basic sites. Thus, it is not surprising that the doping efficiency of BF3 is lower than that of BCF.

Bearing all of the above results in mind, we formulated a hypothesis for the mechanism of p-type doping by BCF that involves

neither adduct formation with the polymers nor ICT to the Lewis acid. Because BCF forms an adduct with PCPDTPT but does not form an adduct with PCPDTBT, our mechanistic studies focus on the latter, for simplicity's sake. The proposed doping mechanism is outlined in Fig. 4. First, a highly acidic (Brønsted-type) BCF-H₂O complex protonates the CPDT moiety of the backbone, generating a negatively charged [BCF:OH]⁻ complex and a positively charged polymer backbone [PCPDTBT-H]⁺.

Second, a neutral chain segment transfers an electron to the positively charged segment, resulting in a neutral, protonated radical species [PCPDTBT-H]• and a positively charged radical species [PCPDTBT]•+. Although we have indicated in Fig. 4 that electron transfer is an intermolecular process, it could very well be an intramolecular process. The negatively charged [BCF:OH]- complex acts as the counter-ion to the positively charged radical of the polymer backbone [PCPDTBT]•+, the species we attribute to being the free charge carriers observed in our electrical measurements.

BCF is known to strongly complex with water, and the resulting Brønsted acidity of the complex is well documented in the literature^{33–38}. To demonstrate this Brønsted acidity, we investigated protonation of the CPDT monomer by BCF and TFA via solution-state ¹H nuclear magnetic resonance (NMR) in dry CDCl₃ (spectra shown in Supplementary Figs. 20–24). Despite the use of dry solvent, preparation of samples in an inert atmosphere glovebox and use of custom air-free NMR tubes, proton resonance observed in neat BCF clearly demonstrates that water is present in sufficient quantity to initiate the doping process. These results, also supported by DFT calculations (Supplementary Fig. 25), demonstrate unequivocally that BCF is capable of protonating CPDT. Previous work also noted the Brønsted basicity of CPDT³⁹. Only a very small amount of doping was detectable by EPR (Supplementary Fig. 26) and UPS (Supplementary Fig. 27).

We compared the UV-Vis-NIR spectroscopic changes of PCPDTBT in dry chlorobenzene following the addition of various amounts of BCF and TFA, as shown in Fig. 5a,b, respectively, and found those changes to be essentially identical. EPR measurements (Supplementary Fig. 28) show that doping occurs in solution, not just in the solid state. Doping of PCPDTBT in the solid state by TFA was also observed by UV-Vis-NIR absorbance (Supplementary Fig. 29), EPR (Supplementary Fig. 30), electrical conductivity (Supplementary Fig. 31) and impedance spectroscopy. At 0.02 molar equivalents of TFA we observed a doping efficiency of 0.1% for PCPDTBT. These data, in conjunction with the NMR experiments, suggest that the inferior doping efficiency of TFA is attributable to its weaker Brønsted acid strength (Supplementary Fig. 32).

In Fig. 5c we show that the direct addition of water to a solution of BCF and PCPDTBT increases the amount of polaron absorption in the NIR region, in support of the proposed doping mechanism. The chlorobenzene solvent was initially dry, suggesting that water had been inadvertently introduced into the sample despite taking all precautions to exclude it (solutions prepared in an inert atmosphere glovebox with the water concentration <1.0 ppm and using oven-dried glassware). Alternative attempts to completely exclude the presence of water were only partially successful (Supplementary Fig. 33). The intentional reintroduction of water to the sublimed BCF resulted in increasing polaron absorption (Supplementary Fig. 34). No spectroscopic changes were observed when excess water was added to PCPDTBT in chlorobenzene (Supplementary Fig. 35). It is worth noting that the doping efficiencies reported from electrical measurements were calculated assuming that the dopant species is BCF, and not the BCF-H2O complex. Because Fig. 5c demonstrates that not all BCF molecules are initially complexed to water, we can conclude that the doping efficiencies of Lewis acids reported in this work are underestimated.

To probe the nature of the radical species present in a mixture of PCPDTBT and BCF, we pursued DFT calculations in conjunction

Step 1: Protonation

Step 2: Electron transfer

Fig. 4 | **Proposed doping mechanism of PCPDTBT by BCF.** Formation of the BCF- H_2O complex is assumed to have already taken place by step 1.

with continuous-wave electron-nuclear double resonance (ENDOR) spectroscopy. Hyper-fine structure could not be resolved from X-band EPR measurements (Supplementary Fig. 36). We chose to simulate the structure of PCPDTBT by modelling an oligomer of four repeat units in length (4-mer), in line with previous studies on

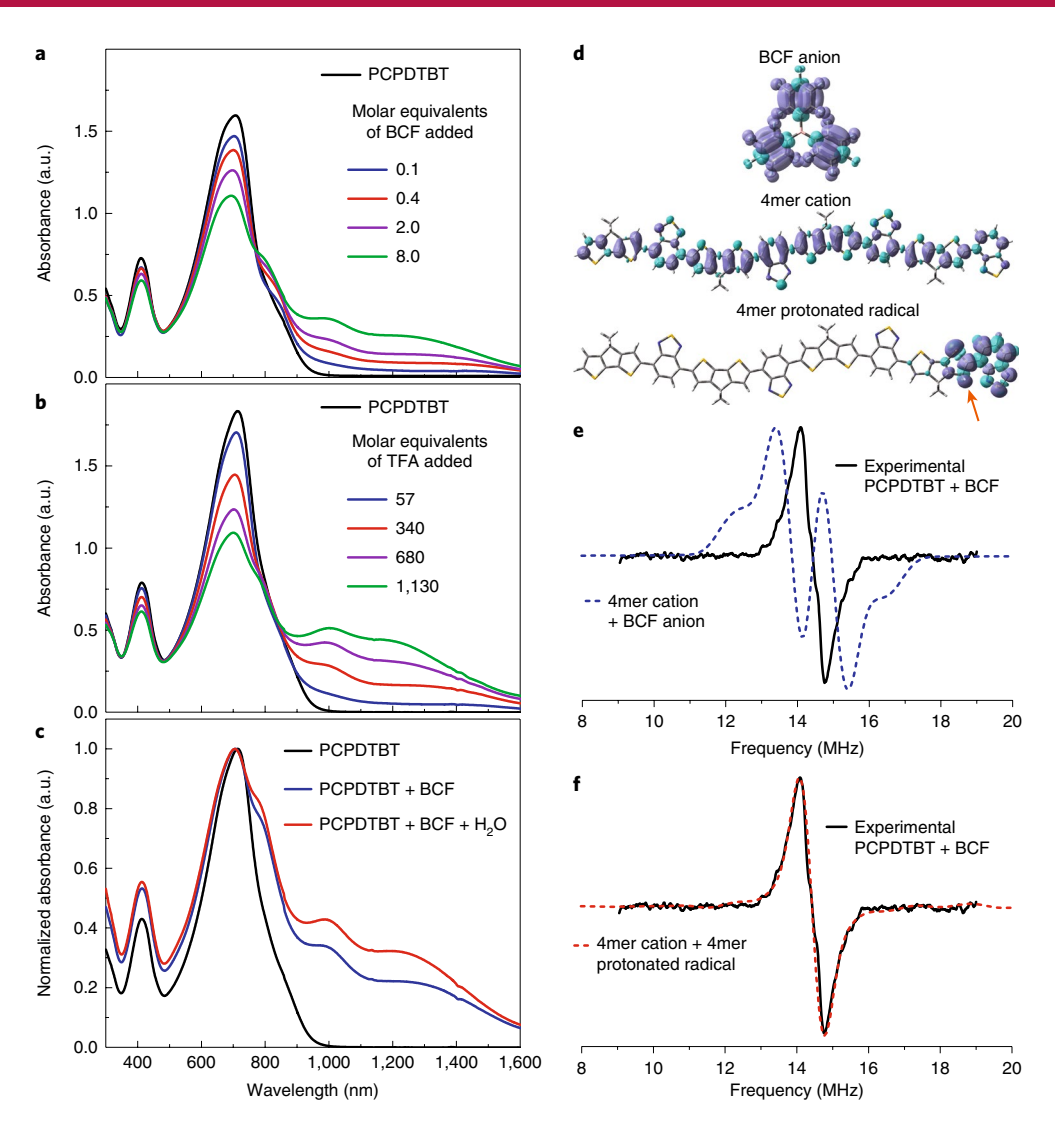


Fig. 5 | Experimental evidence for the proposed doping mechanism of PCPDTBT by BCF. a,b, Absorption in dry chlorobenzene of PCPDTBT with BCF (a) and TFA (b). c, The normalized absorption of PCPDTBT after the sequential addition of 2.0 molar equivalents of BCF and 2.0 molar equivalents of H₂O. d, Spin density isosurface plots for the radical species of interest (contour level of 0.0004 electrons bohr⁻³). e,f, The site of protonation is indicated by the orange arrow. Experimental ENDOR spectrum of PCPDTBT with 1.0 molar equivalents of BCF compared to the simulated spectra.

semiconducting polymers⁴⁰. Further details on the computational methods used herein can be found in Methods. Figure 5d shows the calculated spin densities for the species of interest projected onto their optimized geometries. Note how the spin density of the 4-mer protonated radical is not fully de-localized along the backbone. This suggests that the protonated radical is not a highly mobile species—most probably it is somewhat confined to the region of protonation.

In Fig. 5e,f the experimental ENDOR signal of PCPDTBT with 1.0 mol ar equivalents of BCF is plotted against the results of the ENDOR simulations for ICT and for our proposed doping mechanism (Fig. 4). The simulated results are the 1:1 addition of ENDOR spectra for the radical species indicated. The individual simulated spectra are shown in Supplementary Figs. 37 and 38. These results strongly support our proposed doping mechanism, while also negating the likelihood of ICT. Our DFT calculations suggest that electron transfer after protonation is energetically favourable by about 0.2 eV (Supplementary Fig. 39).

Next, we sought to investigate the efficacy of various Lewis acids at doping a polymer lacking Lewis basic nitrogen atoms altogether, so that adduct formation does not convolute their relative doping efficiencies. For this study, we chose the polymer

poly[(4,4-dihexadecyl-4*H*-cyclopenta[1,2-*b*:5,4-*b*']dithiophene-2,6-diyl)-alt-(2,5-difluoro-1,4-phenylene)] (PhF2,5), whose chemical structure is shown in Fig. 6a (ref. ⁴¹). The sulfur atoms of CPDT are not substantially Lewis basic (Supplementary Fig. 40). In Fig. 6b, changes in the optical absorption of PhF2,5 in chlorobenzene are shown with 8.0 molar equivalents of various Lewis acids, as well as with 116 molar equivalents of TFA for reference. As such, we attribute the increased absorption in the red and NIR regions (700–1100 nm) to polaron absorption, which was corroborated by EPR measurements (Supplementary Fig. 41).

From the absorbance spectra, we can place the four Lewis acids into two categories: strongly doping and weakly doping. BCF and BF₃ fall into the former category, which is consistent with literature noting the Brønsted acidity of water–Lewis acid complexes and the stability of the negatively charged [OH:Lewis acid] complex⁴². Both BBr₃ and aluminium trichloride (AlCl₃) fall into the latter category. Because both of these Lewis acids are known to decompose in the presence of water (Al–Cl and B–Br bond cleavage), they may not be able to form a stable adduct with water and/or the corresponding stable conjugate base^{43,44}. We speculate that the strong proton–fluorine interactions of BCF and BF₃ in their complexes with water,

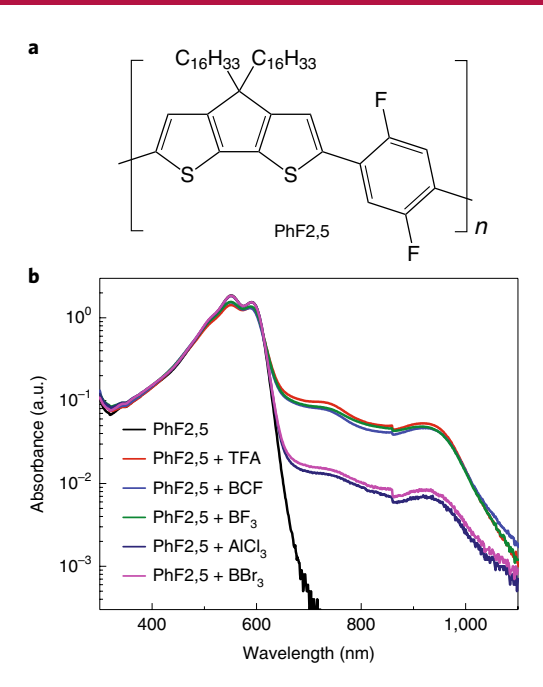


Fig. 6 | Lewis acid doping of a polymer lacking Lewis basic nitrogen atoms. a, Molecular structure of PhF2,5. **b**, Absorption in chlorobenzene of PhF2,5 with 8.0 molar equivalents of various Lewis acids, displayed on a semi-log plot for clarity.

shown in Supplementary Fig. 42, may contribute to the stability and acidity of the complexes, besides, of course, their known resistance to B–C and B–F bond cleavage, respectively^{43,45}.

It is worth noting that Lewis acids in the strongly doping category (BCF, BF₃) are weaker Lewis acids than those in the weakly doping category (BBr₃, AlCl₃)⁴⁶. If the Lewis acids doped by ICT, then one would expect that the stronger Lewis acids, which have greater electron affinity, would be the more effective dopants.

In this work we have thoroughly investigated the p-type doping of organic semiconducting polymers by various Lewis acids. Interestingly, we find that adduct formation is detrimental to the doping efficiency of the Lewis acid. Furthermore, we show that Lewis acid strength does not correlate with its propensity for doping conjugated materials.

A comprehensive investigation into the previously unknown doping mechanism of BCF reveals that doping occurs in two steps: first, a BCF-H₂O complex protonates a CPDT moiety of the polymer backbone. Second, electron transfer takes place from a neutral chain segment to a protonated one. Our combined ENDOR measurements and DFT calculations provide evidence of the precise nature of the radical species produced after protonation, a substantial contribution toward understanding the mechanism of protonic acid doping in polymers.

A survey of the literature indicates that, for the materials which have been shown to be doped by BCF, a structurally recurring theme is the presence of a thiophene-related moiety in the doped material^{18–21,47–49}. In principle, however, any conjugated material with sufficient Brønsted basicity should be able to be doped by Lewis acids. Another limiting factor is expected to be the ionization potential of the conjugated material⁴. Therefore, the development of superior acid dopants ought to focus on improving Brønsted acidity, which does not necessarily involve the use of Lewis acids.

Online content

Any methods, additional references, Nature Research reporting summaries, source data, statements of code and data availability and

associated accession codes are available at https://doi.org/10.1038/s41563-019-0479-0.

Received: 11 May 2019; Accepted: 10 August 2019; Published online: 16 September 2019

References

- Chiang, C. K. et al. Electrical conductivity in doped polyacetylene. Phys. Rev. Lett. 39, 1098–1101 (1977).
- MacDiarmid, A. G. & Heeger, A. J. Organic metals and semiconductors: the chemistry of polyacetylene, (CH)x, and its derivatives. Synth. Met. 1, 101–118 (1980).
- McQuillan, B., Street, G. B. & Clarke, T. C. The reaction of hf with polyacetylene. I. Electron. Mater. 11, 471–490 (1982).
- Han, C. C. & Elsenbaumer, R. L. Protonic acids: generally applicable dopants for conducting polymers. Synth. Met. 30, 123–131 (1989).
- Mai, C.-K. et al. Facile doping of anionic narrow-band-gap conjugated polyelectrolytes during dialysis. Angew. Chem. Int. Ed. 52, 12874–12878 (2013).
- Patil, A. O. et al. Self-doped conducting polymers. Synth. Met. 20, 151–159 (1987).
- Chayer, M., Faid, K. & Leclerc, M. Highly conducting water-soluble polythiophene derivatives. *Chem. Mater.* 9, 2902–2905 (1997).
- Blochwitz, J., Pfeiffer, M., Fritz, T. & Leo, K. Low voltage organic light emitting diodes featuring doped phthalocyanine as hole transport material. *Appl. Phys. Lett.* 73, 729–731 (1998).
- Salzmann, I., Heimel, G., Oehzelt, M., Winkler, S. & Koch, N. Molecular electrical doping of organic semiconductors: fundamental mechanisms and emerging dopant design rules. Acc. Chem. Res. 49, 370–378 (2016).
- Walzer, K., Maennig, B., Pfeiffer, M. & Leo, K. Highly efficient organic devices based on electrically doped transport layers. *Chem. Rev.* 107, 1233–1271 (2007).
- 11. Yim, K.-H. et al. Controlling electrical properties of conjugated polymers via a solution-based p-type doping. *Adv. Mater.* **20**, 3319–3324 (2008).
- Sivaramakrishnan, S. et al. Solution-processed conjugated polymer organic p-i-n light-emitting diodes with high built-in potential by solution- and solidstate doping. Appl. Phys. Lett. 95, 213303 (2009).
- Gao, W. & Kahn, A. Controlled P-doping of zinc phthalocyanine by coevaporation with tetrafluorotetracyanoquinodimethane: a direct and inverse photoemission study. *Appl. Phys. Lett.* 79, 4040–4042 (2001).
- Zhang, Y., de Boer, B. & Blom, P. W. M. Controllable molecular doping and charge transport in solution-processed polymer semiconducting layers. *Adv. Funct. Mater.* 19, 1901–1905 (2009).
- Gao, J. et al. The effect of 2,3,5,6-tetrafluoro-7,7,8,8-tetracyanoquinodimethane charge transfer dopants on the conformation and aggregation of poly(3hexylthiophene). J. Mater. Chem. C 1, 5638–5646 (2013).
- E. Jacobs, I. et al. Comparison of solution-mixed and sequentially processed P3HT:F4TCNQ films: effect of doping-induced aggregation on film morphology. J. Mater. Chem. C 4, 3454–3466 (2016).
- Scholes, D. T. et al. Overcoming film quality issues for conjugated polymers doped with F4TCNQ by solution sequential processing: hall effect, structural, and optical measurements. J. Phys. Chem. Lett. 6, 4786–4793 (2015).
- Zalar, P. et al. Increased mobility induced by addition of a Lewis acid to a Lewis basic conjugated polymer. Adv. Mater. 26, 724–727 (2014).
- 19. Panidi, Julianna et al. Remarkable enhancement of the hole mobility in several organic small-molecules, polymers, and small-molecule:polymer blend transistors by simple admixing of the Lewis acid P-dopant B(C6F5)3. *Adv. Sci.* 5, 1700290 (2017).
- Pingel, P. et al. P-type doping of poly(3-hexylthiophene) with the strong Lewis acid tris(pentafluorophenyl)borane. Adv. Electron. Mater. 2, 1600204 (2016).
- 21. Han, Y. et al. Doping of large ionization potential indenopyrazine polymers via Lewis acid complexation with tris(pentafluorophenyl)borane: a simple method for improving the performance of organic thin-film transistors. *Chem. Mater.* 28, 8016–8024 (2016).
- Welch, G. C., Coffin, R., Peet, J. & Bazan, G. C. Band gap control in conjugated oligomers via Lewis acids. J. Am. Chem. Soc. 131, 10802–10803 (2009).
- 23. Welch, G. C. & Bazan, G. C. Lewis acid adducts of narrow band gap conjugated polymers. *J. Am. Chem. Soc.* 133, 4632–4644 (2011).
- Zalar, P., Henson, Z. B., Welch, G. C., Bazan, G. C. & Nguyen, T.-Q. Color tuning in polymer light-emitting diodes with Lewis acids. *Angew. Chem.* 124, 7613–7616 (2012).
- Randell, N. M., Fransishyn, K. M. & Kelly, T. L. Lewis acid-base chemistry of 7-azaisoindigo-based organic semiconductors. ACS Appl. Mater. Interfaces 9, 24788-24796 (2017)
- Liang, Z., Boland, M. J., Butrouna, K., Strachan, D. R. & Graham, K. R. Increased power factors of organic-inorganic nanocomposite thermoelectric materials and the role of energy filtering. *J. Mater. Chem. A* 5, 15891–15900 (2017).

- Dai, A. et al. Enhanced charge-carrier injection and collection via lamination of doped polymer layers p-doped with a solution-processible molybdenum complex. Adv. Funct. Mater. 24, 2197–2204 (2014).
- Ratcliff, E. L., Lee, P. A. & Armstrong, N. R. Work function control of hole-selective polymer/ITO anode contacts: an electrochemical doping study. J. Mater. Chem. 20, 2672–2679 (2010).
- Li, J. et al. Introducing solubility control for improved organic P-type dopants. Chem. Mater. 27, 5765–5774 (2015).
- J. Lawrence, E., S. Oganesyan, V., G. Wildgoose, G. & E. Ashley, A. Exploring the fate of the tris(pentafluorophenyl)borane radical anion in weakly coordinating solvents. *Dalton Trans.* 42, 782–789 (2013).
- Kwaan, R. J., Harlan, C. J. & Norton, J. R. Generation and characterization of the tris(pentafluorophenyl)borane radical anion. *Organometallics* 20, 3818–3820 (2001).
- 32. Piers, W. E. The chemistry of perfluoraryl boranes. *Adv. Organomet. Chem.* **52**, 1–76 (2005).
- Siedle, A. R., Newmark, R. A., Lamanna, W. M. & Huffman, J. C. Structure of a zirconoxyborane having a zirconium-fluorine-carbon bridge. *Organometallics* 12, 1491–1492 (1993).
- Danopoulos, A. A. et al. Equilibria in the B(C6F5)3–H2O system: synthesis and crystal structures of H2O·B(C6F5)3 and the anions [HOB(C6F5)3]– and [(F5C6)3B(μ-OH)B(C6F5)3]–. Chem. Commun. 0, 2529–2560 (1998).
- 35. Kalamarides, H. A., Iyer, S., Lipian, J., Rhodes, L. F. & Day, C. Pentafluoroaryl transfer from tris(pentafluorophenyl)boron hydrate to nickel. Synthesis and X-ray crystal structure of (PPh2CH2C(O)Ph)Ni(C6F5)2. *Organometallics* 19, 3983–3990 (2000).
- 36. Beringhelli, T., Maggioni, D. & D'Alfonso, G. 1H and 19F NMR investigation of the reaction of B(C6F5)3 with water in toluene solution. *Organometallics* **20**, 4927–4938 (2001).
- Guidotti, S. et al. Synthesis and reactivity of (C6F5)3B-N-heterocycle complexes. 1. Generation of highly acidic Sp3 carbons in pyrroles and indoles. J. Org. Chem. 68, 5445-5465 (2003).
- Focante, F., Mercandelli, P., Sironi, A. & Resconi, L. Complexes of tris(pentafluorophenyl)boron with nitrogen-containing compounds: synthesis, reactivity and metallocene activation. *Coord. Chem. Rev.* 250, 170–188 (2006).
- Tang, T., Lin, T., Wang, F. & He, C. A new aspect of cyclopentadithiophene based polymers: narrow band gap polymers upon protonation. *Chem. Commun.* 51, 13229–13232 (2015).
- Niklas, J. et al. Highly-efficient charge separation and polaron delocalization in polymer-fullerene bulk-heterojunctions: a comparative multi-frequency EPR and DFT study. *Phys. Chem. Chem. Phys.* 15, 9562–9574 (2013).
- Wang, M. et al. Hole mobility and electron injection properties of D-A conjugated copolymers with fluorinated phenylene acceptor units. *Adv. Mater.* 29, 1603830 (2017).
- 42. Wamser, C. A. Equilibria in the system boron trifluoride—Water at 25°. J. Am. Chem. Soc. 73, 409–416 (1951).
- Skinner, H. A. & Smith, N. B. The heat of hydrolysis of boron tribromide. Trans. Faraday Soc. 51, 19–22 (1955).
- Bottero, J. Y., Cases, J. M., Fiessinger, F. & Poirier, J. E. Studies of hydrolyzed aluminum chloride solutions. 1. Nature of aluminum species and composition of aqueous solutions. J. Phys. Chem. 84, 2933–2939 (1980).
- E. Piers, W. & Chivers, T. Pentafluorophenylboranes: from obscurity to applications. Chem. Soc. Rev. 26, 345–354 (1997).
- Beckett, M. A., Brassington, D. S., Coles, S. J. & Hursthouse, M. B. Lewis acidity of tris(pentafluorophenyl)borane: crystal and molecular structure of B(C6F5)3-OPEt3. *Inorg. Chem. Commun.* 3, 530–533 (2000).

- Lee, J. et al. A planar cyclopentadithiophene–benzothiadiazole-based copolymer with Sp2-hybridized bis(alkylsulfanyl)methylene substituents for organic thermoelectric devices. *Macromolecules* 51, 3360–3368 (2018).
- 48. Yan, H. et al. Lewis acid doping induced synergistic effects on electronic and morphological structure for donor and acceptor in polymer solar cells. *Adv. Energy Mater.* **8**, 1703672 (2018).
- Poverenov, E., Zamoshchik, N., Patra, A., Ridelman, Y. & Bendikov, M. Unusual doping of donor-acceptor-type conjugated polymers using lewis acids. J. Am. Chem. Soc. 136, 5138–5149 (2014).

Acknowledgements

This work was supported by the Department of Energy under Award No. DE-SC0017659. D.X.C. was supported by the National Science Foundation Graduate Research Fellowship Program under grant no. 1650114. Any opinions, findings and conclusions or recommendations expressed in this material are those of the authors and do not necessarily reflect the views of the National Science Foundation. D. Leifert was supported by the Alexander von Humboldt Foundation (Feodor Lynen Return Fellowship). XPS, UPS and EPR were obtained at a facility supported by the MRSEC programme of the NSF foundation (no. DMR-1121053). We acknowledge support from the Center for Scientific Computing from the CNSI for the DFT calculations (no. NSF CNS-1725797). This research used beamline 7.3.3 of the Advanced Light Source, which is a DOE Office of Science User Facility under contract no. DE-AC02-05CH11231. T.L. and K.R.G. contributed the UPS and IPES measurements under work supported by the U.S. Department of Energy, Office of Science, Office of Basic Energy Sciences and the EPSCoR programme, under award no. DE-SC0018208. A.E.M. and N.K. acknowledge support by the DFG (FoMEDOS—Projektnummer 286798544). V.V.B. would like to thank J. Vollbrecht for help in processing data, and A. Lill for preparation of substrates with interdigitated contacts.

Author contributions

B.Y. wrote the paper, proposed the mechanism, took all NMR, EPR and ENDOR measurements and performed the DFT calculations. B.Y. helped with absorption spectroscopy measurements. D.X.C. performed XPS and UPS measurements and helped write the manuscript. V.V.B. performed the electrical measurements and helped with writing. D. Leifert synthesized PCPDTPT and helped with absorption spectroscopy. M.W. synthesized PhF2,5. A.D. helped with absorption spectroscopy and GIWAXS. M.S. collected GIWAXS. A.E.M. and D. Lungwitz helped with XPS. T.L. and K.R.G. contributed IPES and UPS. P.J.S. performed the AFM measurements. N.K supervised XPS and helped with the writing. G.C.B. and T.-Q.N. supervised the project and helped with the writing.

Competing interests

The authors declare no competing interests.

Additional information

Supplementary information is available for this paper at https://doi.org/10.1038/s41563-019-0479-0.

 $\textbf{Reprints and permissions information} \ is \ available \ at \ www.nature.com/reprints.$

Correspondence and requests for materials should be addressed to G.C.B. or T.-Q.N.

Supplementary Information Additional data from electrical measurements, method for determining free charge carrier density, spectroscopic data, AFM images and computational results.

Publisher's note: Springer Nature remains neutral with regard to jurisdictional claims in published maps and institutional affiliations.

© The Author(s), under exclusive licence to Springer Nature Limited 2019

Methods

BCF was purchased from Tokyo Chemical Industry Co., Ltd. and used as received. BF $_3$ (diethylether), BBr $_3$ (1 M in dichloromethane), AlCl $_3$, TFA and the solvents used herein were purchased from Sigma-Aldrich and used as received. PCPDTBT was purchased from 1-Material and used as received. PCPDTPT was synthesized in-house according to a published procedure 50 . F $_4$ TCNQ was purchased from Lumtec and used as received. All materials were stored in a dry, inert atmosphere (N $_2$) glovebox. Careful precautions were taken to exclude the presence of water and oxygen during all measurements and sample preparation, except where indicated.

Thin films of the polymers with dopants were prepared by making a concentrated solution ($\sim\!20\,\text{mg}\,\text{ml}^{-1}$) in chloroform with the appropriate amount of dopant, allowing the solution to equilibrate for at least 12 h and then spin-cast onto the appropriate, clean substrate.

Conductivity measurements. Direct current electrical conductivity of pristine and doped polymer films (0.002, 0.005, 0.01, 0.02 mol l-¹ BCF and BF₃) was measured using interdigitated gold contacts photolithographically prepared on silicon dioxide (SiO₂). The width and length of the channel were 20 cm and 8 μm, respectively. The thickness of the gold contacts was 50 nm. The polymer films were spin-cast on pre-cleaned substrates with the interdigitated gold contacts from a chloroform solution (5 mg ml⁻¹) at a spin speed of 2,000 r.p.m. Current (I)-voltage (V) characteristics were measured using a semiconductor analyser (Keithley 4200). Electrical conductivity was calculated as σ =(L/Wd)×(dV/dI), where L=8 μ m is the length of the channel, W=20 cm is the width of the channel and d=50 nm is the thickness of the film.

UPS. Measurements were obtained using a Kratos Axis Ultra DLD XPS system under vacuum (10^{-8} Torr) using He I line with 21.21-eV photons (Supplementary Figs. 12 and 13). Samples were prepared on freshly cleaned conductive indium tin oxide/glass substrates at a thickness of approximately 10 nm. The films were mounted onto a sample bar using double-sided adhesive tape, electrically ground to the sample bar using nickel impregnated tape and biased at -9 V.

Impedance spectroscopy. Measurements were obtained from a device structure of n⁺⁺-Si/SiO₂(200 nm)/benzocyclobutene (BCB, 30 nm)/active layer/Au to create the MIS architecture. Benzocyclobutene was spun-cast on top of the SiO₂ dielectric layer from a 1 mg ml⁻¹ solution at 4,000 r.p.m. and then annealed at 250 °C for 1h. The active layer was spin-coated at 1,200 r.p.m. on top of BCB after cooling, followed by thermal evaporation of the gold contact. The n⁺⁺-Si was used as the working electrode. The stack of 200-nm SiO₂ and 20−30-nm BCB served as the insulator layer. Film thickness measurements were carried out using an Innova AFM. MIS devices were analysed using a Solartron 1260 impedance analyser. The impedance spectra were measured over a wide frequency range (10 Hz−3 MHz) with a small alternating current amplitude signal of 20 mV and various direct current biases ranging from −15 to 20 V. The method for determining the number of free charge carriers (p) from these measurements is described in Supplementary information.

GIWAXS. Measurements we taken at beamline 7.3.3 of the Advanced Light Source with an X-ray wavelength of 1.2398 Å ($10\,\mathrm{keV}$) at a sample–detector distance of 274 mm. Measurements were calibrated using an Ag-behenate standard. Samples were scanned in a He environment at an incidence angle of 0.12°. Diffraction patterns were processed using the Nika software package for Wavemetrics Igor, in combination with a custom Igor script, WAXStools.

AFM. All AFM images reported in this study were obtained in tapping mode on an Asylum MFP-3D set-up using a Pt/Cr-coated silicon tip (Budget Sensors) with a resonance frequency of 75 kHz and a force constant of 3 N m⁻¹. All images were obtained using a 0.40-Hz scan rate at a 90° scan angle to account for tip geometry.

UV-Vis-NIR absorption. Spectra were obtained using a Perkin-Elmer Lambda 750 UV-Vis-NIR spectrometer. Thin films were prepared on cleaned glass substrates and encapsulated inside a glovebox using epoxy and another glass substrate. After curing, the samples were measured outside the glovebox. For solution absorption, the concentrations of PCPDTPT and PCPDTBT were always 0.025 and 0.05 mg ml⁻¹, respecticely. The concentration of PhF2,5 for solution absorption was always 0.025 mg ml⁻¹.

EPR. Measurements were taken on a Bruker EMXplus Spectrometer System in continuous-wave mode in the X-band frequency (9.3 GHz) using a Bruker ER 4119HS-LC high-sensitivity resonator. The microwave cavity was tuned each time a new sample was loaded. Quartz capillaries (1.0 inner diameter) were used to hold the samples. For each set of experiments indicating the intensity of the EPR signal, the sample was adjusted in the cavity to maintain Qvalues within 10% of each other. Error bars of 20% are included to account for both variations in the Qvalue and potential fluctuations in the amount of solution loaded by capillary action into the quartz tubes, despite every precaution having been taken to maintain identical

sample preparation identical. Solid-state samples were prepared by drawing up a concentrated solution of the polymer $(20\,\mathrm{mg\,ml^{-1}})$ with the appropriate amount of dopant, and letting the solvent evaporate in a glovebox over the course of 24 s. Both ends were capped with Critoseal before removal from the glovebox and measurement immediately. For solution-state measurements, the concentration of polymer was maintained at a constant $0.125\,\mathrm{mg\,ml^{-1}}$ in chlorobenzene.

XPS. Measurements were obtained using a Kratos Axis Ultra DLD XPS under vacuum (10^{-9} Torr) using monochromated X-rays produced using an aluminium source running at a potential of $14\,\mathrm{kV}$ and a current of $14\,\mathrm{mA}$. A pass energy of 20 was used for all high-resolution element sweeps, and 160 for survey sweeps. Sample preparation was identical to that described for UPS measurements. Peak fitting was performed using WINSPEC, and atomic sensitivity factors for each element were taken into account during peak integrations.

IPES and UPS. UPS measurements were performed in a PHI 5600 ultra-high vacuum system comprising an 11-inch-diameter hemispherical electron energy analyser and a multi-channel plate detector (Supplementary Fig. 20). UV photons were generated from an Excitech H Lyman-α lamp (E-LUX121) coupled to a 90° ellipsoidal mirror (E-LUXTM EEM Optical Module) with a high-purity dried oxygen purge of the beam path at 8-9 Torr. A bias of -5 V was applied to all samples for UPS measurements, and the pass energy was 2.95 eV. IPES spectra were captured using the Bremsstrahlung isochromat mode with electron kinetic energy <5 eV to reduce sample damage. Samples were biased at -20 V. During all IPES measurements, the UHV chamber was kept in the dark to avoid interference from external light. The low-energy electron beam source was a Kimball Physics ELG-2 electron gun equipped with a low-temperature (1,150 K) barium oxide cathode. Generated photons were focused with a fused silica bi-convex lens and detected with an optical bandpass filter (214 or 280 nm) coupled to a photomultiplier tube (R585, Hamamatsu Photonics). IPES for PCDTBT with 0.5 and 1.0 molar equivalents of BCF were measured using a 214-nm bandpass filter (Andover Corp.) due to high electron affinity, while other samples were measured using a 280-nm bandpass filter (Semrock). All IPES measurements were operated with a custom LabView programme.

ENDOR. Experimental continuous-wave ENDOR was acquired on a Bruker EMXplus Spectrometer System fitted with an ENDOR probehead (Bruker EN 801 resonator). A solution of PCPDTBT (20 mM in chloroform with respect to the repeat unit) with 1.0 molar equivalents of BCF was prepared in a glovebox using an airtight quartz EPR tube (outer diameter 5 mm). The sample was removed from the glovebox, flash-frozen in liquid nitrogen and maintained at 100 K during measurements. The microwave power and frequency were 6.3 mW and 9.5 GHz, respectively, and the magnetic field strength was 3,390 G. The radio frequency power was attenuated by 10 dB. ENDOR spectra were simulated from DFT calculations using the EasySpin software. A magnetic field strength of 3,390 G and linewidth 0.8 MHz (full width at half-maximum, Gaussian broadening) were used as parameters of the simulation. First-order perturbation theory was used to speed up the calculations. In regard to the oligomeric structures of PCPDTBT, the magnetic properties of alkyl protons and the two terminal aromatic protons were not considered. This was done to better reflect the physical nature of the polymer.

DFT. Gaussian09 was used for DFT geometry optimization at the B3LYP/6-31 G(d,p) level of theory. Solubilizing alkyl chains were replaced by methyl groups to expedite calculations. The conductor-like polarizable continuum model, CPCM, was used to investigate the energetics of proton transfer and electron transfer (solvent, chlorobenzene). The coordinates of the optimized geometries were then used as a starting point for DFT calculation of magnetic properties (g-tensors and hyper-fine coupling constants) using the ORCA computational package. Magnetic properties were calculated using the B3LYP functional and EPR-II basis set (except for sulfur atoms, which used the def2-TZVPP basis set) in vacuo. The anisotropic magnetic dipole and isotropic Fermi contact contributions to hyper-fine coupling constants were calculated only for aromatic protons of the 4-mer, excluding the two terminal protons (one on each end) of the oligomer. For BCF, contributions from only boron and fluorine were considered. This approach (neglecting the effect of solvent, replacing alkyl chains with methyl groups, choice of oligomeric length and so on) for calculation of magnetic properties using DFT methods is described and justified in more detail in ref. 40.

Data availability

The main data supporting the findings of this study are available within the Article and Supplementary Information files. Additional data are available from the corresponding authors on request.

References

 Ying, L. et al. Regioregular pyridal[2,1,3]thiadiazole π-conjugated copolymers. J. Am. Chem. Soc. 133, 18538–18541 (2011).